Multipartite entanglement in the random Ising chain

Jay S. Zou and Helen S. Ansell
Department of Physics and Astronomy, Northwestern University, Evanston, Illinois 60208, USA

István A. Kovács*
Department of Physics and Astronomy, Northwestern University, Evanston, Illinois 60208, USA
and Northwestern Institute on Complex Systems, Northwestern University, Evanston, Illinois 60208, USA

(Received 8 June 2022; accepted 22 July 2022; published 2 August 2022)

Quantifying entanglement of multiple subsystems is a challenging open problem in interacting quantum systems. Here, we focus on two subsystems of length ℓ separated by a distance $r = \alpha\ell$ and quantify their entanglement negativity ($\mathcal{E}$) and mutual information ($\mathcal{I}$) in critical random Ising chains. We find universal constant $\mathcal{E}(\alpha)$ and $\mathcal{I}(\alpha)$ over any distances, using the asymptotically exact strong disorder renormalization group method. Our results are qualitatively different from both those in the clean Ising model and random spin chains of a singlet ground state, like the spin-$\frac{1}{2}$ random Heisenberg chain and the random XX chain. While for random singlet states $\mathcal{I}(\alpha)/\mathcal{E}(\alpha) = 2$, in the random Ising chain this universal ratio is strongly α dependent. This deviation between systems contrasts with the behavior of the entanglement entropy of a single subsystem, for which the various random critical chains and clean models give the same qualitative behavior. The reason is that $\mathcal{E}$ and $\mathcal{I}$ are sensitive to higher order correlations in the ground-state structure. Therefore, studying multipartite entanglement provides additional universal information in random quantum systems, beyond what we can learn from a single subsystem.

DOI: 10.1103/PhysRevB.106.054201

I. INTRODUCTION

Entanglement is a distinguishing property of quantum mechanics, offering fundamentally stronger correlations than classical physics. In quantum many-body systems, studying the entanglement properties is a promising way to understand universal properties, in particular the vicinity of quantum phase transitions [1–4]. In this paper, we show that quantifying multipartite entanglement provides additional universal information, by distinguishing entanglement patterns that appear to be qualitatively the same when considering only a single subsystem.

Generally, the entanglement between a subsystem, A and the rest of the system, B, in the ground state, $|\Psi\rangle$, is quantified by the von Neumann entropy of the reduced density matrix, $\rho_A = \mathrm{Tr}_B|\Psi\rangle\langle\Psi|$ as

$$\mathcal{S}_A = -\mathrm{Tr}_A(\rho_A \log_2 \rho_A). \tag{1}$$

In one-dimensional systems we have an almost complete understanding [5–7]: $\mathcal{S}_A$ is known to diverge logarithmically at a quantum critical point as $\mathcal{S}_A = \frac{c}{3}\log_2 \ell + cst$. Here ℓ is the size of the subsystem and the prefactor is universal, with c being the central charge of the conformal field theory. These results have been extended to further properties, including the Rényi entropy and the properties of the entanglement spectrum [8]. Qualitatively similar results have been obtained for quantum models in the presence of quenched disorder [9–11]. In random chains (random antiferromagnetic Heisenberg and XX models, random Ising model [RIM], etc.) the critical point is controlled by a so-called infinite disorder fixed point [12,13], the properties of which can be conveniently studied by the strong disorder renormalization group (SDRG) method [14,15]. Using the SDRG, a logarithmic entanglement entropy is found with a universal prefactor [10], which has been numerically checked by density-matrix renormalization [4] and by free-fermionic methods [16]. It is not a coincidence that various random chains show similarities, as indicated by the exact relationship between the entanglement entropy of the random XX chain and the RIM [17]. Another mapping revealed the underlying random singlet (RS) representation of the ground state of the RIM in terms of $\mathrm{SU}(2)_2$ particles [18], extending the results in Ref. [10]. Overall, quantum entanglement of a single interval is qualitatively similar in all these critical quantum systems. The question arises, whether this similarity extends to the entanglement properties of multiple intervals. In other words, do we gain new, universal information about critical quantum systems by quantifying multipartite entanglement? Here, we show that the answer is positive: The multipartite entanglement structure is qualitatively different in these otherwise similar systems. The reason is that multipartite entanglement is sensitive to additional patterns, e.g., higher order correlations, that the entanglement entropy is agnostic to. The main finding of our results is that such higher order patterns are universal in the right scaling limit.

Multipartite entanglement is challenging to quantify, even in small quantum systems [19]. The entanglement entropy

*Corresponding author: istvan.kovacs@northwestern.edu

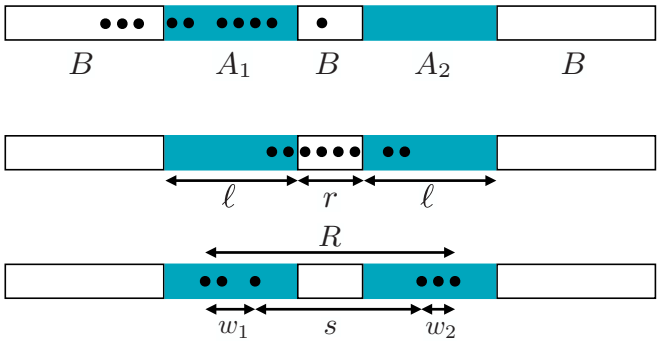

FIG. 1. We consider a tripartition of the system into two subsystems A_1 and A_2, and the rest of the system B. The subsystems each have length ℓ and are separated by a distance r. Top: schematic of a cluster in the RIM that does not contribute to $\mathcal{I}$ or $\mathcal{E}$. Middle: a cluster that contributes only to $\mathcal{I}$. Bottom: a cluster that contributes to both $\mathcal{I}$ and $\mathcal{E}$; see text for details.

is only suitable when the two subsystems span the entire system. Here, we consider two computable measures, the entanglement negativity ($\mathcal{E}$) and mutual information ($\mathcal{I}$) across multiple subsystems (two distant intervals A_1, A_2 and the rest of the system, B); see Fig. 1. Note that B is generally disconnected, as it consists of two or three intervals, depending on the boundary conditions. $\mathcal{I}$ is given by

$$\mathcal{I} = \mathcal{S}_{A_1} + \mathcal{S}_{A_2} - \mathcal{S}_{A_1\cup A_2}, \tag{2}$$

while $\mathcal{E}$ is quantified by the logarithmic negativity

$$\mathcal{E} = \ln \mathrm{Tr}\left|\rho^{T_2}_{A_1\cup A_2}\right|, \tag{3}$$

where $\rho^{T_2}_{A_1\cup A_2}$ is the partially transposed reduced density matrix with respect to A_2, given by $\langle\phi_1\phi_2|\rho^{T_2}_{A_1\cup A_2}|\phi_1'\phi_2'\rangle \equiv \langle\phi_1\phi_2'|\rho_{A_1\cup A_2}|\phi_1'\phi_2\rangle$. Here, $\{\phi_1\}$ and $\{\phi_2\}$ are bases for A_1 and A_2, respectively. $\mathcal{E}$ is an entanglement monotone and it also serves as an upper bound for the distillable entanglement, although it is notoriously difficult to compute in practice [20–25]. In contrast, $\mathcal{I}$ accounts for both classical and quantum correlations, so a nonzero value does not necessarily mean quantum entanglement.

Multipartite entanglement has been studied in random quantum chains that exhibit an RS phase, where the ground state factorizes into singlets, each composed of two spins; see, for example, the random XX chain and random antiferromagnetic spin-1/2 Heisenberg (XXX) chain [26]. In such random chains in the RS phase, $\mathcal{I}$ and $\mathcal{E}$ provide the same information as $\mathcal{I}/\mathcal{E} = 2$, due to the simple entanglement structure, as shown by SDRG and free-fermionic techniques [26]. Here, we show that this is not true in general, as in the RIM $\mathcal{E}$ and $\mathcal{I}$ behave qualitatively differently, both capturing additional information compared to $\mathcal{S}$.

The RIM is given by the Hamiltonian

$$\mathcal{H} = -\sum_{\langle ij\rangle} J_{ij}\sigma_i^x\sigma_j^x - \sum_i h_i\sigma_i^z, \tag{4}$$

in terms of the $\sigma_i^{x,z}$ Pauli matrices at sites i of a one-dimensional chain. The nearest neighbor couplings, J_{ij}, and the transverse fields, h_i, are independent non-negative random numbers, taken from some nonsingular distributions, to be specified later. As far as universal properties are concerned, the shape of the distributions is irrelevant. The ground state of the RIM is conveniently determined by an efficient SDRG algorithm [27]. During the SDRG method [15], the largest local terms in the Hamiltonian in Eq. (4) are successively eliminated and new Hamiltonians are generated through perturbation calculation. The critical properties of the RIM are governed by an infinite disorder fixed point, in which the strength of disorder grows without limit during renormalization [13]. Therefore, the SDRG results are asymptotically exact in the vicinity of the critical point, which is indeed demonstrated both analytically [28,29] and numerically [30,31]. After decimating all degrees of freedom, the ground state of the RIM is found as a collection of independent ferromagnetic clusters of various size, each cluster being in a GHZ state $\frac{1}{\sqrt{2}}(|\uparrow\uparrow\ldots\uparrow\rangle + |\downarrow\downarrow\ldots\downarrow\rangle)$.

II. CLUSTER COUNTING IN THE RIM

For a single subsystem, each GHZ cluster contributes $\log_2 2 = 1$ to the entanglement entropy [Eq. (1)] if the cluster has at least one site inside and one site outside of the subsystem, otherwise the contribution is 0 [10]. Thus, calculation of the entanglement entropy for the RIM is equivalent to a cluster counting problem. Here, we study $\mathcal{I}$ and $\mathcal{E}$ between two subsystems of size ℓ, separated by distance r, with total system size L, shown in Fig. 1. From Eq. (2), it readily follows that calculating $\mathcal{I}$ also leads to a cluster counting problem. Let us indicate the number of specific cluster configurations by $C_{x_1yx_2}$, where $x_i = 1$ if the cluster has some sites in subsystem A_i, and $y = 1$ if it has sites in B, while both x_i and y are 0 otherwise. Then, $\mathcal{S}_{A_1} = C_{110} + C_{101} + C_{111}$, $\mathcal{S}_{A_2} = C_{011} + C_{101} + C_{111}$, while $\mathcal{S}_{A_1\cup A_2} = C_{011} + C_{110} + C_{111}$, leading to

$$\mathcal{I} = 2C_{101} + C_{111}. \tag{5}$$

As $\mathcal{E}$ is additive on tensor products, independent magnetic clusters contribute additively. For $\mathcal{E}$, a nonvanishing contribution requires a cluster that has sites in both A_1 and A_2, while no sites outside [26]. Independently from the number of spins in the GHZ state, $\mathcal{E}$ is the same as for a Bell state, which will have one negative eigenvalue of $-1/2$ after performing the partial transpose. Hence, $\mathcal{E}$ is the result of another cluster counting problem, $\mathcal{E} = C_{101}$, leading to

$$\mathcal{I} = 2\mathcal{E} + C_{111}. \tag{6}$$

Interestingly, $\mathcal{I} - \mathcal{E} = C_{101} + C_{111}$ has the simplest geometric interpretation: the total number of clusters that have sites in both subsystems. Note that $C_{111} = 0$ when clusters have only two sites, which is the case for the previously studied systems in the RS phase, leading to $\mathcal{I} = 2\mathcal{E}$ [26]. In contrast, clusters in the RIM can have a large number of sites, yielding a nonzero C_{111}, breaking the simple proportionality of $\mathcal{I}$ and $\mathcal{E}$. At this point, it is not even clear if $\mathcal{I}$ or $\mathcal{E}$ (or their ratio) remain universal in the RIM.

III. ANALYTIC RESULTS

The SDRG has been used to provide the leading-order scaling of the entanglement entropy for one subsystem [9], corresponding to an effective central charge. Due to cluster

counting, there is an underlying geometric interpretation

$$\mathcal{S}(L,\ell)=\frac{1}{L}\sum_{s=1}^{L/2}n(s)\min(\ell,s), \tag{7}$$

where $n(s)$ is the number of instances in all clusters of gap-size s, defined as the distance between consecutive sites in the same cluster [11,32], with periodic boundary conditions this is given by $s=\min(x_{i+1}-x_i, L-x_{i+1}+x_i)$. The reason behind Eq. (7) is that one site of each gap needs to be outside of the subsystem, while the other site needs to be inside. Therefore, each gap of size $s>\ell$ contributes to ℓ positions of the subsystem, while a gap of size $s<\ell$ contributes to s positions. For an illustration, see Fig. 11 of Ref. [11]. For large L, the summation in Eq. (7) can be approximated by an integral, yielding the leading-order universal logarithmic scaling $S(L,\ell)=\frac{1}{6}\ln\ell$, as $n(s)=Cs^{-2}$ for large L and $C/L=c_{\rm eff}/(3\ln 2)=\frac{1}{6}$ for the RIM [9].

Based on the known gap-size statistics $n(s)$, a strict bound can also be calculated for $\mathcal{E}$ and $\mathcal{I}$. In practice, $\mathcal{E}$ and $\mathcal{I}$ are averaged over a large number of random samples as well as for all L subsystem positions in each sample. First, we consider configurations where the subsystems are positioned in a way that the sites of the gap fall inside separate subsystems. This can happen only when $s>r$ in a cluster. Such a configuration has *at least* 1 contribution to $\mathcal{I}$ (2 if it has no sites in B, i.e., C_{101}), while *at most* 1 contribution to $\mathcal{E}$ (0 if it has sites in B, i.e., C_{111}). Out of all L potential subsystem locations, there are $s-r$ (if $s<\ell+r$), or $2\ell+r-s$ (if $s\geqslant\ell+r$) such configurations. Hence, the bound is

$$\mathcal{B}=\frac{C}{L}\int_r^{\ell+r}ds\frac{s-r}{s^2}+\frac{C}{L}\int_{\ell+r}^{2\ell+r}ds\frac{2\ell+r-s}{s^2}. \tag{8}$$

$\mathcal{B}$ is a lower bound for $\mathcal{I}$ and an upper bound for $\mathcal{E}$. Performing the integrals and using $C/L=c_{\rm eff}/(3\ln 2)$, which is valid for both the critical RIM and critical RS states, yields

$$\mathcal{B}(x)=-\frac{c_{\rm eff}}{3\ln 2}\ln(1-x). \tag{9}$$

Here x is the scale-invariant cross ratio $x=\ell^2/(\ell+r)^2$, or in general

$$x=\frac{\ell_1\ell_2}{(\ell_1+r)(\ell_2+r)}, \tag{10}$$

when the two subsystems have different lengths, ℓ_1 and ℓ_2. In an RS state, where each cluster has two sites, the bound captures $\mathcal{E}$ exactly for large L, $\mathcal{B}=\mathcal{E}=\mathcal{I}/2$, as shown independently in Ref. [26]. In the case when $r=\alpha\ell$ and $\ell_1=\ell_2=\ell$, the bound is a distance-independent constant that only depends on α (Fig. 4):

$$\mathcal{B}(\alpha)=-\frac{c_{\rm eff}}{3\ln 2}\ln\left(1-\frac{1}{(1+\alpha)^2}\right). \tag{11}$$

Note that recently, in the RS phase, finite-size corrections to $n(s)$ have been characterized, also offering a way to calculate corrections to $\mathcal{B}$ [33]. In comparison, clusters in the RIM often contain more than two sites. As illustrated in Fig. 1, a contributing gap is surrounded by a total linear extent of the cluster of length w_1 and w_2 on each side. Therefore, in the RIM the α dependence of $\mathcal{E}$ and $\mathcal{I}$ can be different from each other as well as from that of $\mathcal{B}(\alpha)$, as discussed in more detail in the Appendix. In general, $\mathcal{E}$ and $\mathcal{I}$ depend on higher order correlations in the ground state. As an exact result, $\mathcal{E}$ can be written as

$$\begin{aligned}\mathcal{E}=\int_0^{\ell}dw_1\int_0^{w_1}dw_2\Bigg[&\int_r^{\ell+r-w_1}ds\,p_{s,w_1,w_2}\frac{s-r}{L}\\&+\int_{\ell+r-w_1}^{2\ell+r-w_1-w_2}ds\,p_{s,w_1,w_2}\frac{\ell-w_1}{L}\\&+\int_{\ell+r-w_2}^{2\ell+r-w_1-w_2}ds\,p_{s,w_1,w_2}\frac{\ell+r-s-w_2}{L}\Bigg],\end{aligned} \tag{12}$$

where p_{s,w_1,w_2} stands for the number of (s,w_1,w_2) triplets in a sample. This result highlights why the RS representation of the RIM in Ref. [18] leads to results that deviate from those observed in RS states. While $\mathcal{S}$ is only sensitive to the $n(s)=\int dw_1\int dw_2 p_{s,w_1,w_2}$ gap-size statistics, which is the same as in RS states, $\mathcal{E}$ depends on the full p_{s,w_1,w_2} statistics (see Fig. 7), including the linear extent of the cluster on both sides of each gap, w_i.

IV. NUMERICAL RESULTS

We have studied critical RIM chains up to subsystem size $\ell=8192$ with at least 10 000 realizations for each size, using periodic boundary conditions. Following Refs. [34,35], we have used two different ferromagnetic disorder distributions, in both of which J_{ij} is uniformly distributed in [0, 1]. For *box-h* disorder, the distribution of the transverse fields is uniform in $[0,h]$, whereas for *fixed-h* disorder we have $h_i=h$, $\forall i$. The quantum control parameter is defined as $\theta=\ln(h)$, and the critical point is located at $\theta_{\rm box}=0$ and $\theta_{\rm fixed}=-1$, respectively.

Here, we present our results for the linear case, when $r=\alpha\ell$, with $\alpha=2^n$, sampled for $n=-5,-4,\ldots,1$. The system size L would ideally be much larger than $\ell\to\infty$. Numerical SDRG studies for the entanglement entropy of a single subsystem of size ℓ have shown that $L=2\ell$ is sufficiently large in practice [32]. Therefore, we chose ℓ such that the total linear extent of the boundaries of the two subsystems $2\ell+r$ spans half of the system, i.e., $L=2(2\ell+r)$. The finite-size estimates of $\mathcal{I}$ and $\mathcal{E}$ in the linear case are shown

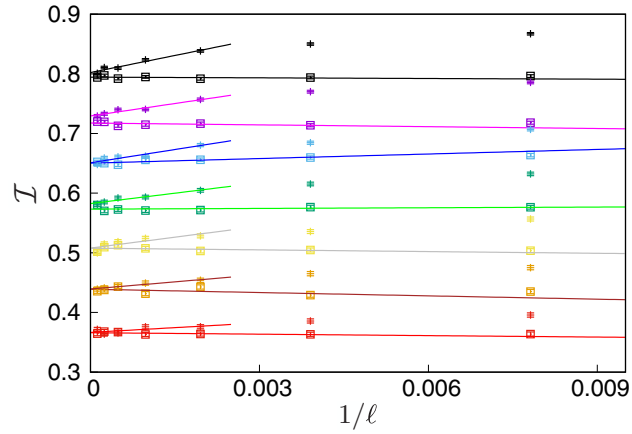

FIG. 2. $\mathcal{I}$ in the RIM for $\alpha=2^n$, with $n=-5,-4,\ldots,1$ from top to bottom for fixed-h (+) and box-h (□) disorder distributions.

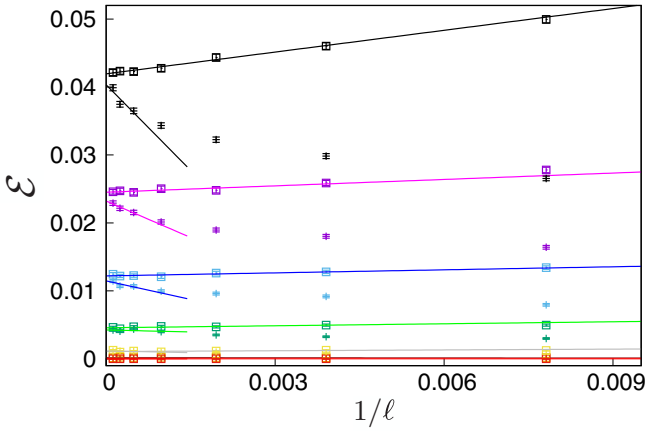

FIG. 3. The same as Fig. 2 for $\mathcal{E}$. Interestingly, the finite-size corrections are of opposite sign compared to $\mathcal{I}$. For box-h disorder, the linear extrapolation fits the data in the entire range of sizes for both $\mathcal{I}$ and $\mathcal{E}$.

in Figs. 2 and 3, extrapolated to infinite size as $1/\ell \to 0$. For both $\mathcal{I}$ and $\mathcal{E}$, the extrapolated values agree for the two disorder distributions, indicating universality. Our main results are summarized in Fig. 4, illustrating the universal $\mathcal{E}$ and $\mathcal{I}$ values for the studied values of α. We observe that $\mathcal{I}$ and $\mathcal{E}$ are very different from each other, as well as from $\mathcal{B}$. In stark contrast to random quantum chains of a critical RS state, in the RIM the ratio of $\mathcal{I}$ and $\mathcal{E}$ depends on α. Interestingly, in the studied range of α, $\mathcal{I}$ appears to decay linearly as $\mathcal{I} = a - b\ln\alpha$, with $a = 0.438(1)$ and $b = 0.102(1)$. However, as $\mathcal{I}$ is positive and larger than $\mathcal{B}$, there must be deviations from this expression for larger values of $\alpha \approx 50$. To support our numerical findings, an approximate argument for the α dependence is presented in the Appendix, providing Eq. (A1), which was used in the fit in Fig. 4. The use of $\mathcal{I} - \mathcal{E}$ as a proxy for $\mathcal{I}$ is justified by the fact that in the observed range $\mathcal{E}$ is much smaller than the upper bound provided by $\mathcal{B}$; see the Appendix for supporting analytic arguments.

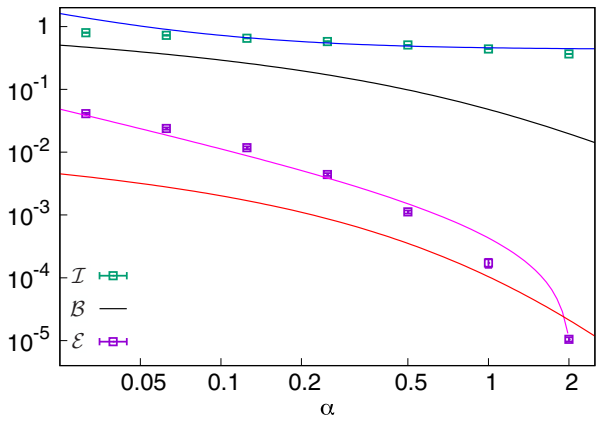

FIG. 4. The extrapolated ($1/\ell \to 0$) $\mathcal{I}$ and $\mathcal{E}$ values, averaged over the two disorder distributions, box-h and fixed-h, as a function of $\alpha = r/\ell$, together with the analytic bound $\mathcal{B}$. As $\mathcal{I} \gg \mathcal{E}$, $\mathcal{I}$ can be fitted by Eq. (A1) (blue line). $\mathcal{E}$ is fitted by two different approximations, given by Eq. (A2) (magenta), as well as Eq. (A4) (red). In each case, the indicated error bars are smaller than the size of the symbol.

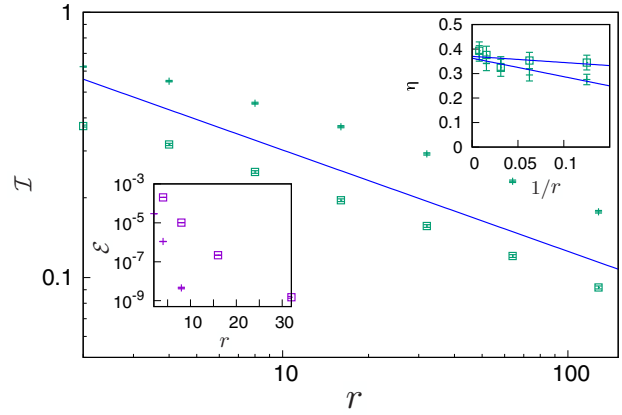

FIG. 5. $\mathcal{I}$ in the RIM for finite $\ell = 2$ for fixed-h (+) and box-h (□) disorder distributions. Upper inset: Two-point estimates of the η exponent are compatible with the analytic SDRG result $\eta = \frac{3-\sqrt{5}}{2} \approx 0.382$ (illustrated by the blue line in the main panel). Lower inset: $\mathcal{E}$ in the RIM for $\ell = 2$.

V. FINITE INTERVALS

For finite ℓ, the value of $\mathcal{B}$ is no longer universal, but asymptotically decays as a power law with a universal exponent

$$\mathcal{B} = \frac{c_{\text{eff}}}{3\ln 2}\frac{\ell^2}{r(2\ell + r)} \sim r^{-2}, \tag{13}$$

which has been checked numerically both with SDRG and DMRG in the RS state [26]. In the RIM, $\mathcal{E}$ is not expected to be universal, as the probability $p(r)$ of a small cluster surviving decimation up to a length scale r depends heavily on the initial disorder distribution. Two such, independent, surviving clusters can connect with a finite probability in the SDRG procedure, resulting in the nonuniversal expectation $\mathcal{E} \sim (p(r))^2$. In line with this expectation, our numerical results are illustrated in the lower inset of Fig. 5, indicating fast, nonuniversal decay.

As for $\mathcal{I} - \mathcal{E}$, we expect qualitatively different behavior than $\mathcal{B}(r) \sim r^{-2}$ in the RS phase. For $\ell = 1$, $\mathcal{I} - \mathcal{E}$ is the (longitudinal) two-point correlation function of two spins being in the same cluster. At the critical point, such correlations decay algebraically, with the same exponent for any finite ℓ, $\mathcal{I} - \mathcal{E} \sim r^{-\eta}$ for $r \gg \ell$, where $\eta = \frac{3-\sqrt{5}}{2} \approx 0.382$ according to SDRG results [12,13]. The value of η has been also confirmed by numerical calculations using free-fermionic techniques [30,31]. Our numerical SDRG results for $\ell = 2$ are in line with this theoretical expectation (Fig. 5), as both $\mathcal{I}$ and $\mathcal{I} - \mathcal{E}$ are found to decay algebraically with a universal exponent $\eta = 0.37(2)$.

VI. DISCUSSION

We presented our results for two multipartite entanglement measures $\mathcal{E}$ and $\mathcal{I}$ in critical RIM chains between subsystems of size ℓ, separated at a distance r. Our results indicate a linear scaling limit ($r = \alpha\ell$) for critical quantum correlations, where multipartite entanglement approaches distance-independent universal values for $\mathcal{E}$ and $\mathcal{I}$. Our results differ qualitatively

from those known in critical RS states (e.g., random antiferromagnetic Heisenberg and XX models), where $\mathcal{I}/\mathcal{E} = 2$. In the RIM, the ratio of $\mathcal{I}$ and $\mathcal{E}$ is still universal but depends strongly on α, indicating that the two measures capture different universal aspects of the underlying correlations. The strong deviation from the simple RS results is due to the more complex ground-state structure in the RIM and is expected to be a generic feature of critical quantum systems that are not in an RS state. We have shown that the RS results serve as a lower bound for $\mathcal{I}$ and an upper bound for $\mathcal{E}$. In general, tripartite entanglement is related to coarse-grained three-point correlation functions. Our results indicate that the corresponding integrated statistics [i.e., Eq. (12)] is universal in the linear scaling limit. While we provided quantitative arguments that fit the α dependence of $\mathcal{E}$ and $\mathcal{I}$ in the RIM more closely than the RS results, it remains an open challenge to calculate $\mathcal{E}$ and $\mathcal{I}$ analytically, similarly to the already established calculation of the entanglement entropy [10]. A potentially promising direction is through the well-known mapping to a random potential representation of the SDRG treatment, similarly to the application in Ref. [36].

In addition to the linear scaling limit, there are several other possibilities to consider. A simple case is for adjacent intervals when $r = 0$ but $\ell \propto L$. However, this limit does not provide additional information compared to a single subsystem. For both the RIM and models in the RS state, $\mathcal{E}(\ell) = \mathcal{S}(\ell)/2$, as the same cluster contributions are encountered as for $\mathcal{S}$, over one endpoint out of the two endpoints of the subsystem. We have also explored the case of finite subsystems (constant ℓ when $r \to \infty$) and found a nonuniversal $\mathcal{E}$, while the decay of $\mathcal{I}$ is universal and the same as the known SDRG result of the two-point correlation function. In sum, characterizing multipartite entanglement between large *nonadjacent* subsystems is a promising strategy to gain additional insights into quantum criticality compared to single subsystem studies. We note that $\mathcal{I}$ and $\mathcal{E}$ are expected to behave differently outside of the critical point. While both $\mathcal{I}$ and $\mathcal{E}$ have to vanish in the paramagnetic phase, in the ferromagnetic phase only $\mathcal{E}$ is expected to vanish, while $\mathcal{I} = 1$ for large sizes, as there is a giant magnetic domain.

Our investigations can be extended in several directions. Here, we mention further quantum chains both with and without disorder, as well as interacting quantum systems in higher dimensions [32,37–39], and systems with long-range interactions [40–42]. The mutual information ($\mathcal{I}$) results can be readily extended to more subsystems, $A_1, \ldots, A_n$, $n > 2$, potentially leading to even more pronounced differences between various models. For $n > 2$, $\mathcal{I}$ is zero in RS states, while nonzero and presumably universal in the RIM. Finally, we mention nonequilibrium dynamics of $\mathcal{E}$ and $\mathcal{I}$ after a quench, i.e., a sudden change of the parameters in the Hamiltonian at time $t = 0$ [43].

ACKNOWLEDGMENTS

We thank Z. Zimborás and R. Juhász for helpful discussions. We would like to acknowledge the WCAS Summer Grant Award from the Weinberg College Baker Program in Undergraduate Research at Northwestern University.

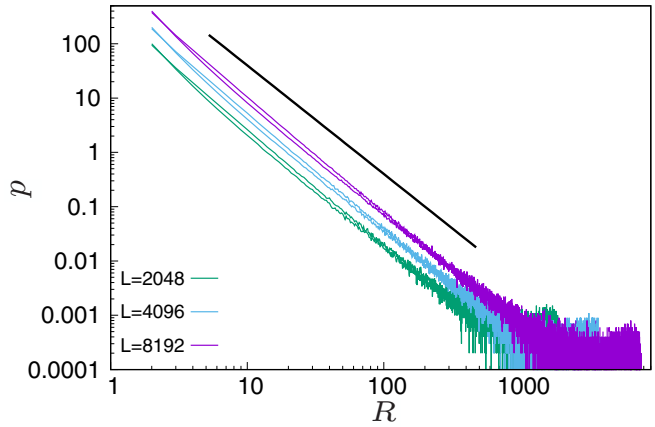

FIG. 6. Distribution of the linear extent R of the clusters averaged over 10 000 samples. For each size, we show two lines, corresponding to the box-h and fixed-h distributions, respectively. The black line has a slope of -2, illustrating our approximation $p_R \sim LR^{-2}$.

APPENDIX

Here, we present two arguments when $r = \alpha L$ as an attempt to better capture $\mathcal{E}(\alpha)$ and $\mathcal{I}(\alpha)$ than the $\mathcal{B}$ bound in Eq. (11).

1. Estimating $\mathcal{I} - \mathcal{E}$

$\mathcal{I} - \mathcal{E} = C_{101} + C_{111}$ has a contribution in at most $R - r$ positions out of L for each cluster of linear extent $R > r$; see Fig. 1 for an illustration. SDRG suggests that there can be only $O(L/R)$ such large clusters. Hence, the position averaged $\mathcal{I} - \mathcal{E}$ is expected to be proportional to $1 - r/R$ for each such cluster ($R > r$), the probability of which is given by p_R. Hence,

$$\mathcal{I} - \mathcal{E} \propto \int_r^L dR\, p_R \left(1 - \frac{r}{R}\right) \sim a + b\left(\beta + \frac{1}{\beta}\right), \qquad \text{(A1)}$$

with $\beta \equiv \frac{r}{L} = \frac{\alpha}{2(2+\alpha)}$. Based on numerical observations (see Fig. 6), we used $p_R \sim LR^{-2}$ to estimate the integral. The best fit is given by $a = 0.41(3)$ and $b = 0.007(2)$.

2. Estimating $\mathcal{E}$

Depending on the shape of the cluster (given by s, w_1, and w_2), there are three distinct configurations to consider that contribute to $\mathcal{E}$. For two equal-sized subsystems of length ℓ, we can choose to label the cluster such that $w_1 \geqslant w_2$ without loss of generality. The three contributing cases are as follows:

(1) When the range of contributing positions is dictated by s. This is the case when $w_1 + s \leqslant \ell + r$ and $w_2 + s \leqslant \ell + r$. There are $s - r$ contributing positions, yielding

$$\int_0^\ell dw_1 \int_0^{w_1} dw_2 \int_r^{\ell+r-w_1} ds\, p_{s,w_1,w_2} \frac{s-r}{L}.$$

(2) When the range of contributing positions is dictated by s on one side and w_1 on the other. This is the case when $w_1 + s \geqslant \ell + r$ and $w_2 + s \leqslant \ell + r$. There are $\ell - w_1$ contributing

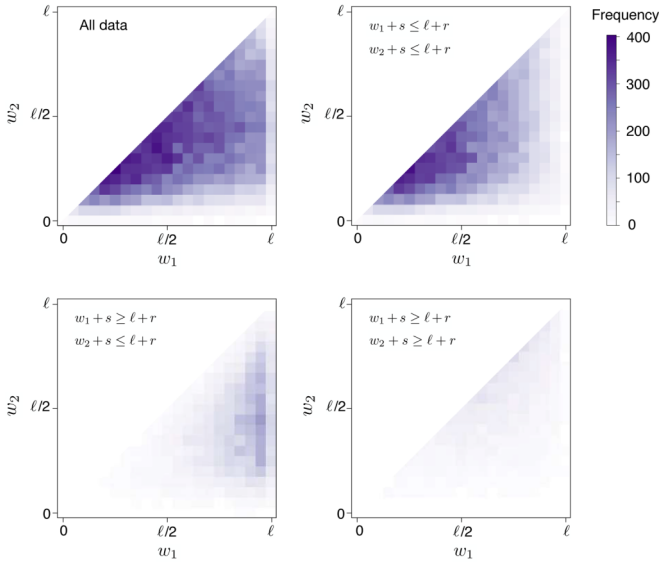

FIG. 7. Frequency distribution of clusters contributing to $\mathcal{E}$ for a system with $L = 8\,192$, at $\alpha \approx 1/2$, which corresponds to $\ell = 1638.4$ and $r = 819.2$. The w_1 and w_2 values are binned into bins of width 80. The first panel corresponds to all points that contribute to $\mathcal{E}$ (41 966 points). The other three panels correspond to the points that contribute to each of the three cases discussed and have 28 133, 10 213, and 3 620 points respectively for cases 1, 2, and 3. The number of data points within each bin is indicated by the same color scale for each plot.

positions, yielding

$$\int_0^\ell dw_1 \int_0^{w_1} dw_2 \int_{\ell+r-w_1}^{\ell+r-w_2} ds\, p_{s,w_1,w_2} \frac{\ell - w_1}{L}.$$

(3) When the range of contributing positions is dictated by w_1 on one side and w_2 on the other. This is the case when $w_1 + s \geqslant \ell + r$ and $w_2 + s \geqslant \ell + r$ (and $w_1 + w_2 + s \leqslant 2\ell + r$). There are $2\ell + r - s - w_1 - w_2$ contributing positions, yielding

$$\int_0^\ell dw_1 \int_0^{w_1} dw_2 \int_{\ell+r-w_2}^{2\ell+r-w_1-w_2} ds\, p_{s,w_1,w_2} \frac{2\ell+r-s-w_1-w_2}{L}.$$

The sum of these three contributions, Eq. (12), is an exact result for $\mathcal{E}$, assuming that the joint statistics p_{s,w_1,w_2} is known analytically. As this is not the case, we need to rely on approximations of the observed p_{s,w_1,w_2} counts, illustrated in Fig. 7. As we have cluster contributions only when $w_1, w_2 \leqslant \ell$ and $s \geqslant r$, along with $r = \alpha\ell$, we find that the relevant range is $w_1, w_2 \leqslant s/\alpha$.

As a first approximation, we can estimate $w_1 = \eta_1 s/\alpha$ and $w_2 = \eta_2 s/\alpha$, yielding

$$\frac{c_{\text{eff}}}{3\ln 2}\left[\ln\left(\frac{(1+\alpha)(\alpha+\eta_2)}{(\alpha+\eta_1)^2}\right) + \frac{\alpha+\eta_1+\eta_2}{\alpha}\ln\left(\frac{(1+\alpha)(\alpha+\eta_1+\eta_2)}{(2+\alpha)(\alpha+\eta_2)}\right)\right]. \quad \text{(A2)}$$

Fitting this to the numerical data, we find $\eta_1 = 0.87(1)$ and $\eta_2 = 0.86(1)$, as shown in Fig. 4. While such a fit works in the studied range of α, it goes negative for larger α. Ideally, we would need an estimate of p_{s,w_1,w_2} that stays positive for any α.

As a second approximation, we assume that w_i are independent from each other as well as from s, and carry out the s integral first, yielding

$$\int_0^\ell dw_1 p_{w_1} \int_0^{w_1} dw_2 p_{w_2} \mathcal{B}(x), \quad \text{(A3)}$$

where x depends on w_1 and w_2, through $\ell_1 = \ell - w_1$ and $\ell_2 = \ell - w_2$ in Eq. (10). This result is intuitive as it indicates that additional sites in the cluster reduce the number of contributing positions by effectively reducing the size of the subsystems by the amount w_i. Assuming a box distribution for both w_1 and w_2 leads to

$$\frac{1}{(2+\alpha)^2}\left[2(1+\alpha)(3+\alpha)\ln\left(\frac{1+\alpha}{\alpha}\right) - (2+\alpha)^2\ln\left(\frac{2+\alpha}{\alpha}\right) - 1\right], \quad \text{(A4)}$$

up to an overall multiplicative constant. In Fig. 4, we show Eq. (A4) fitted to the data, with the constant numerically determined. While the fit is less good than the first approximation over the range of α values investigated, Eq. (A4) remains positive in the limit $\alpha \to \infty$, scaling as $1/\alpha^4$.

[1] P. Calabrese, J. Cardy and B. Doyon (Eds.), Entanglement entropy in extended quantum systems, J. Phys. A: Math. Theor. **42**, 500301 (2009).

[2] L. Amico, R. Fazio, A. Osterloh, and V. Vedral, Entanglement in many-body systems, Rev. Mod. Phys. **80**, 517 (2008).

[3] J. Eisert, M. Cramer, and M. B. Plenio, Colloquium: Area laws for the entanglement entropy, Rev. Mod. Phys. **82**, 277 (2010).

[4] N. Laflorencie, Scaling of entanglement entropy in the random singlet phase, Phys. Rev. B **72**, 140408(R) (2005).

[5] C. Holzhey, F. Larsen, and F. Wilczek, Geometric and renormalized entropy in conformal field theory, Nucl. Phys. B **424**, 443 (1994).

[6] G. Vidal, J. I. Latorre, E. Rico, and A. Kitaev, Entanglement in Quantum Critical Phenomena, Phys. Rev. Lett. **90**, 227902 (2003).

[7] P. Calabrese and J. Cardy, Entanglement entropy and quantum field theory, J. Stat. Mech. (2004) P06002.

[8] P. Calabrese and A. Lefevre, Entanglement spectrum in one-dimensional systems, Phys. Rev. A **78**, 032329 (2008).

[9] G. Refael and J. E. Moore, Criticality and entanglement in random quantum systems, J. Phys. A: Math. Theor. **42**, 504010 (2009).

[10] G. Refael and J. E. Moore, Entanglement Entropy of Random Quantum Critical Points in One Dimension, Phys. Rev. Lett. **93**, 260602 (2004).

[11] J. A. Hoyos, A. P. Vieira, N. Laflorencie, and E. Miranda, Correlation amplitude and entanglement entropy in random spin chains, Phys. Rev. B **76**, 174425 (2007).

[12] D. S. Fisher, Random Transverse Field Ising Spin Chains, Phys. Rev. Lett. **69**, 534 (1992); Critical Behavior of Random Transverse-Field Ising Spin Chains, Phys. Rev. B **51**, 6411 (1995).

[13] D. S. Fisher, Phase transitions and singularities in random quantum systems, Phys. A **263**, 222 (1999).

[14] S. K. Ma, C. Dasgupta, and C.-K. Hu, Random Antiferromagnetic Chain, Phys. Rev. Lett. **43**, 1434 (1979); C. Dasgupta and S. K. Ma, Low-temperature properties of the random Heisenberg antiferromagnetic chain, Phys. Rev. B **22**, 1305 (1980).

[15] For reviews, see F. Iglói and C. Monthus, Strong disorder RG approach of random systems, Phys. Rep. **412**, 277 (2005); Strong disorder RG approach—a short review of recent developments, Eur. Phys. J. B **91**, 290 (2018).

[16] F. Iglói and Y.-C. Lin, Finite-size scaling of the entanglement entropy of the quantum Ising chain with homogeneous, periodically modulated and random couplings, J. Stat. Mech. (2008) P06004.

[17] F. Iglói and R. Juhász, Exact relationship between the entanglement entropies of XY and quantum Ising chains, EPL **81**, 57003 (2008).

[18] N. E. Bonesteel and K. Yang, Infinite-Randomness Fixed Points for Chains of Non-Abelian Quasiparticles, Phys. Rev. Lett. **99**, 140405 (2007).

[19] Sz. Szalay, Multipartite entanglement measures, Phys. Rev. A **92**, 042329 (2015).

[20] A. Peres, Separability Criterion for Density Matrices, Phys. Rev. Lett. **77**, 1413 (1996).

[21] K. Życzkowski, P. Horodecki, A. Sanpera, and M. Lewenstein, Volume of the set of separable states, Phys. Rev. A **58**, 883 (1998).

[22] K. Życzkowski, Volume of the set of separable states. II, Phys. Rev. A **60**, 3496 (1999).

[23] J. Lee, M. S. Kim, Y. J. Park, and S. Lee, Partial teleportation of entanglement in a noisy environment, J. Mod. Opt. **47**, 2151 (2000); J. Eisert and M. B. Plenio, A comparison of entanglement measures, *ibid.* **46**, 145 (1999).

[24] G. Vidal and R. F. Werner, Computable measure of entanglement, Phys. Rev. A **65**, 032314 (2002).

[25] M. B. Plenio, Logarithmic Negativity: A Full Entanglement Monotone that is not Convex, Phys. Rev. Lett. **95**, 090503 (2005); J. Eisert, Entanglement in quantum information theory, arXiv:quant-ph/0610253.

[26] P. Ruggiero, V. Alba, and P. Calabrese, Entanglement negativity in random spin chains Phys. Rev. B **94**, 035152 (2016).

[27] F. C. Alcaraz, J. A. Hoyos, and R. A. Pimenta, Powerful method to evaluate the mass gaps of free-particle quantum critical systems, Phys. Rev. B **104**, 174206 (2021).

[28] B. M. McCoy and T. T. Wu, Theory of a two-dimensional Ising model with random impurities. I. Thermodynamics, Phys. Rev. **176**, 631 (1968); Theory of a two-dimensional Ising model with random impurities. II. Spin correlation functions, **188**, 982 (1969); B. M. McCoy, Theory of a two-dimensional Ising model with random impurities. III. Boundary effects, *ibid.* **188**, 1014 (1969); Theory of a two-dimensional Ising model with random impurities. IV. Generalizations, Phys. Rev. B **2**, 2795 (1970).

[29] R. Shankar and G. Murthy, Nearest-neighbor frustrated random-bond model in $d = 2$: Some exact results, Phys. Rev. B **36**, 536 (1987).

[30] A. P. Young and H. Rieger, Numerical study of the random transverse-field Ising spin chain, Phys. Rev. B **53**, 8486 (1996).

[31] F. Iglói and H. Rieger, Density Profiles in Random Quantum Spin Chains, Phys. Rev. Lett. **78**, 2473 (1997); Random transverse Ising spin chain and random walks, Phys. Rev. B **57**, 11404 (1998).

[32] I. A. Kovács and F. Iglói, Universal logarithmic terms in the entanglement entropy of 2d, 3d, and 4d random transverse-field Ising models, EPL **97**, 67009 (2012).

[33] R. Juhász, Corrections to the singlet-length distribution and the entanglement entropy in random singlet phases, Phys. Rev. B **104**, 054209 (2021).

[34] I. A. Kovács and F. Iglói, Critical behavior and entanglement of the random transverse-field Ising model between one and two dimensions, Phys. Rev. B **80**, 214416 (2009); Renormalization group study of the two-dimensional random transverse-field Ising model, **82**, 054437 (2010).

[35] I. A. Kovács and F. Iglói, Infinite-disorder scaling of random quantum magnets in three and higher dimensions, Phys. Rev. B **83**, 174207 (2011); Renormalization group study of random quantum magnets, J. Phys.: Condens. Matter **23**, 404204 (2011).

[36] R. Juhász and I. A. Kovács, Population boundary across an environmental gradient: Effects of quenched disorder, Phys. Rev. Research **2**, 013123 (2020).

[37] V. Eisler and Z. Zimborás, Entanglement negativity in two-dimensional free lattice models, Phys. Rev. B **93**, 115148 (2016).

[38] H. Wichterich, J. Vidal and S. Bose, Universality of the negativity in the Lipkin-Meshkov-Glick model, Phys. Rev. A **81**, 032311 (2010).

[39] I. A. Kovács, Quantum multicritical point in the two- and three-dimensional random transverse-field Ising model, Phys. Rev. Research **4**, 013072 (2022).

[40] I. A. Kovács, R. Juhász, and F. Iglói, Long-range random transverse-field Ising model in three dimensions, Phys. Rev. B **93**, 184203 (2016).

[41] R. Juhász, I. A. Kovács, and F. Iglói, Long-range epidemic spreading in a random environment, Phys. Rev. E **91**, 032815 (2015).

[42] R. Juhász, I. A. Kovács and F. Iglói, Random transverse-field Ising chain with long-range interactions, EPL **107**, 47008 (2014).

[43] F. Iglói, Zs. Szatmári and Y.-C. Lin, Entanglement entropy dynamics of disordered quantum spin chains, Phys. Rev. B **85**, 094417 (2012).